Applied Catalysis B: Environmental 156–157 (2014) 273–283

Contents lists available at ScienceDirect

Applied Catalysis B: Environmental

journal homepage: www.elsevier.com/locate/apcatb

Photo-catalytic activity of titanium dioxide carbon nanotube nano-composites modified with silver and palladium nanoparticles

Nomso Hintsho[a], Leslie Petrik[a], Alexander Nechaev[a], Salam Titinchi[a], Patrick Ndungu[b,*]

[a] Environmental and Nanosciences Research Group, Department of Chemistry, University of the Western Cape, Bellville, South Africa
[b] School of Chemistry, University of KwaZulu-Natal, Westville Campus, Durban, South Africa

ARTICLE INFO

Article history:
Received 15 July 2013
Received in revised form 7 March 2014
Accepted 11 March 2014
Available online 20 March 2014

Keywords:
Carbon nanotubes
Titanium dioxide
Methylene blue
Silver nanoparticles
Palladium nanoparticles
Metal-organic chemical vapor deposition

ABSTRACT

Photo-catalytic noble metallic and bimetallic nano-composites (Ag or Pd/-TiO_2/CNT) were synthesized using a commercial source of multi-walled carbon nanotubes via a modified dry-mix metal-organic chemical vapour deposition method (MOCVD). The titania loading was varied from 10–40 wt.%, and the optimum TiO_2/CNT photo-catalyst was determined using methylene blue degradation as a model probe reaction. Furthermore, acid-treated nanotubes and non-acid treated nanotubes were compared as a substrate for the synthesis of various titania nano-composites, and it was found that the acid treatment decreased the photo-catalytic activity of the titania CNT nano-composites. The 20 wt.% titania on CNT samples were then further modified with silver, palladium, and a combination of both metals using the MOCVD technique. It was found that the silver titania CNT nano-composites were the most effective photo-catalyst for the degradation of methylene blue. The deposition of 2% Ag on 20% TiO_2/MWCNT resulted in 92% degradation of 50 mg/L MB in 4 h with 1 g/L of photo-catalyst. Palladium had little effect in altering the photo-catalytic activity of the titania CNT nano-composites, and the combination of both metals suppressed the photo-catalytic activity of the titania CNT nano-composites.

1. Introduction

Carbon nanotubes (CNTs) have some very interesting physical chemical properties that can be exploited with relative ease, especially when they are used as a catalyst support material for a metal or metal oxide of interest. The sp^2 hybridization of the carbon–carbon bonds, and the resultant cylindrical arrangement of the graphene sheets are the underlying fundamental characteristics that define CNT properties. As a result, there has been a wide range of R&D activities that probe and investigate the basic physical–chemical aspects of CNTs, and at the same time numerous authors have applied CNTs in proof of concept devices, or as components of a particular system of interest. These diverse fields of interest include catalysis, biomedical applications, micro/nano-electronics, environmental science, and material science in general.

Titanium dioxide is a well-known photo-catalyst, and some key historical developments with this material are given by Fujishima et al. [1]. Over the years various studies have investigated the use of titanium dioxide as a photo-catalyst to remove dyes and various other organic compounds from water [2–4].

The combination of titanium dioxide with carbon nanomaterials such as graphene [5,6], and CNTs is an interesting and very active area of research [7]. The synergy between the materials has been shown to improve the photo-catalytic process. Liu et al. [8] synthesized titanium dioxide with CNTs, tested the photo-catalytic activity by monitoring the degradation of a basic acridine dye, and determined that the highest activity was with material that had been sintered at 300 °C. Kuo [9], demonstrated that the simple mixing of CNTs and titanium dioxide significantly improved the photo-catalytic degradation process of a reactive red 2 dye, and suggested that the addition of CNTs reduced the recombination rate of electron–hole pairs, and increased the generation of hydroxyl radicals. Xu et al. [10] compared a mechanical mixing method and a wet impregnation route to produce titanium dioxide and CNT composites, and found that the wet impregnation route produced a highly active photo-catalyst for the degradation of methyl orange and phenol. They concluded the CNTs act as stabilising support for the formation of nano-particulate titanium dioxide, and act as an electron reservoir thus hindering electron–hole recombination. Jiang, Zheng, Wang, Li and Sun [11], used a wet deposition method to coat CNTs with titanium dioxide, and after calcinations at 450 °C, produced a photo-catalyst that was more active than titanium dioxide alone, for the degradation methylene blue in the presence of hydrogen peroxide. A wet deposition method was used by Saleh

* Corresponding author. Tel.: +27 31 260 3097: fax: +27 31 260 3091.
E-mail address: ndungup@ukzn.ac.za (P. Ndungu).

http://dx.doi.org/10.1016/j.apcatb.2014.03.021
0926-3373/

and Gupta [12], to produce titanium dioxide-CNT nano-composites. The material was shown to be effective in the degradation of methylene blue (93% degradation versus 65% with TiO_2 only). Recently, Takenaka et al., used linker molecules (urea or glycine amide) during the hydrolysis of titanium isopropoxide in the presence of well dispersed CNTs to produce a uniform coating of titanium dioxide on the CNT walls. The authors effectively showed that the composites and the platinum derivatives (Pt/TiO_2-CNT and TiO_2-CNT@Pt) were effective at degrading acetic acid and other small organic molecules, and the most effective catalysts was the TiO_2-CNT@Pt [13].

Besides the use of CNTs, the photo-catalytic activity of titanium dioxide has been improved by the addition of metals; and of particular interest is the use of Ag and Pd. The advantages and mechanisms behind the enhanced photo-catalytic activity with the addition of noble metal nanoparticles to titanium dioxide have been reviewed in the literature [14–16].

In our current work, we present a simple dry-mix metal-organic chemical vapour deposition (MO-CVD) method to synthesize TiO_2/CNT, and TiO_2/CNT nano-composites modified with Ag, Pd and Ag/Pd. The MO-CVD method eliminates the need for solvents in the synthesis of the various composites, and as such can be considered an environmentally friendly synthesis method for such nano-composites. In addition it is a one-pot method with significantly fewer steps than solution based techniques.

2. Experimental

A dry mix technique was used for the metal-organic chemical vapour deposition (MOCVD) of titanium dioxide on to carbon nanotubes. Multi-walled carbon nanotubes (~50–70 nm diameter, and 30–50 μm length) were purchased from cheap tubes. The MWCNTs had a purity of >98.0 wt.%. All chemicals were purchased from Sigma Aldrich (RSA) and were used without further purification.

Some samples were prepared using pre-treated multi-walled carbon nanotubes (MWCNT). For pre-treatment, 1.0 g of the MCWNTs were refluxed for 120 min (at 110 °C) in a 50.0 mL mixture of analytical grade 98 wt.% sulphuric acid, and 38.0 wt.% nitric acid (volume ratio of 3:1). The nanotubes were then washed with distilled water until the rinse solution reached pH 6–7. The nanotubes were dried overnight an oven at 90 °C.

For the MOCVD process, 1.0 g of the MWCNTs were weighed and transferred to a mortar, and carefully mixed with a pre-weighed amount of titanium oxy acetylacetonate (Ti-acac, 98% purity). The mass of Ti-acac used was calculated using the desired loading of titanium dioxide on the MWCNT as a reference point. The mixed powder was then transferred to a stainless steel CVD reactor. An image of the CVD reactor is presented in Fig. 1(A).

The reactor was sealed and tested for leaks. The CVD reactor was then connected to a vacuum line (evacuation powered by a rotary vacuum pump), and placed in a tube furnace. The reactor was evacuated to a pressure of $\sim 5.8 \times 10^{-1}$ mbar at room temperature and then to a similar final pressure at 100 °C to remove excess water. After 30 min the valve to the reactor was closed, and the temperature was ramped up to 360 °C, and then after 15–20 min the temperature was checked and ramped to 400 °C. After 30 min, the temperature was reset to room temperature, and the CVD reactor was left to cool to room temperature in the tube furnace.

To deposit Ag, Pd, or Ag/Pd onto the TiO_2/CNT nano-composites, a pre-weighed amount of Ag acetylacetonate (97.5% purity), or palladium acetylacetonate (97.5% purity) was mixed with the TiO_2/CNT nano-composites, and subjected to the same MOCVD process described above.

3. Characterization

The samples were characterized using scanning electron microscopy (SEM), High Resolution Transmission Electron Microscopy (HRTEM), X-ray diffraction (XRD), Nitrogen sorption at 77 K, and FTIR. For SEM analysis, a FEI Quanta 200 FEG ESEM instrument equipped with a field emission gun operating under high vacuum conditions at an accelerating voltage of 15 keV was used. Using the SEM, energy dispersive X-ray spectroscopy, qualitative analysis, was done on the samples. The spectra were obtained with a Genesis energy-dispersive X-ray spectrometer at an accelerating voltage of 25 keV. XRD data were collected using a D8 Advanced Brukker AXS X-ray diffractometer with Bragg–Brentano geometry and a Cu-Kα source (40 kV, 40 mA). The HRTEM was conducted on a Technai G2 F 20 X-Twin MAT microscope. Band gap measurements were calculated from the tauc plot of the absorption spectra of the different samples collected using a HR2000+ model High Resolution Ocean Optics spectrometer with a halogen HL-2000-FHSA light source, a T300-RT-UV-VIS EOS 1212277 optical fibre probe, barium sulphate powder as a reference standard, and the Spectra Suite software for capturing

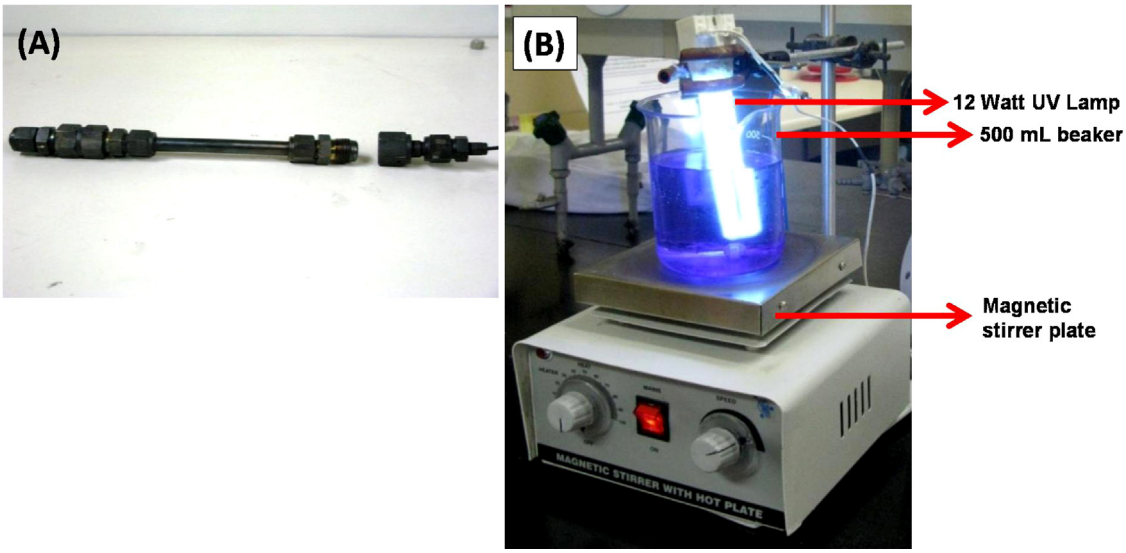

Fig. 1. (A) is an image of the stainless steel CVD reactor used for all synthesis experiments, and (B) is a picture of the set-up used to test photo-catalytic activity of the various nano-composites synthesized. The solution volume used was 500 mL, the stirrer was set at 80 rpm, and the distance beaker size was '500 mL'.

the data. For each sample, ten scans were averaged using an integration time of 15 ms. Photoluminescence (PL) spectra for the nano-composites were collected using a Perkin Elmer LS35 fluorescence spectrometer with a front surface accessory LS55 model solid probe.

4. Photo-catalytic activity

In a typical experiment, a suspension containing the required amount of the catalyst (typically 0.5 g/500 mL) and 500 mL of 50 mg/L aqueous methylene blue solution (prepared with distilled water) was stirred for an hour in the dark at natural pH before irradiation to UV light (12 W UV Lamp). Fig. 1(B) presents an image of the experimental set-up used to test the samples for photo-catalytic activity.

To determine the activity of the catalyst 4 mL of the sample was withdrawn by syringe for analysis. The reaction mixture was stirred for continuous dispersion of the catalyst. The concentration of the methylene blue dye in the dark was used as the initial value for the measurements of methylene blue dye degradation. At each interval of 1 h, a 4 mL sample was withdrawn by syringe from the irradiated solution. The catalyst was separated by filtering from the aqueous solution prior to analysis. The concentration of the methylene blue dye (lambda max 663 nm) in solution was determined using a calibration curve of methylene blue (concentration vs absorbance) prepared with known concentrations using a UV/VIS spectrophotometer. Typical percentage error between sample measurements was 1–3%.

4.1.1. Effect of pH on the photo-catalytic properties of 20 wt.% TiO_2/CNT

The same procedure described above for the test of photo-catalytic activity was followed for the pH experiments, but in this case different solutions of methylene blue were used at different pH values. The catalyst used was the 20% TiO_2/MWCNT (un-oxidized CNTs), the pH range was from 2 to 12, and the solutions pH was adjusted using NaOH or H_2SO_4.

4.1.2. Optimizing treatment time

These were done using similar methods to those described above. The experiments were carried out for 2 to 12 h, the solution was at pH 8, the catalyst used was the 20% TiO_2/MWCNT (un-oxidized CNTs), the concentration of the MB dye was 50 mg/L and amount of photo-catalyst was 0.5 g/500 mL of solution.

4.1.3. Variation of the amount of catalyst used

The basic procedure developed to test the photo-catalytic activity was followed. The amount of catalyst in the solution was varied. The catalyst used was the 20% TIO_2/MWCNT (un-oxidized CNT), and the concentrations were 0.125 g/L; 0.25 g/L; 0.5 g/L; 1 g/L and 2 g/L. The reaction was run for 8 h.

4.1.4. Varying the concentration of the dye

The amount of dye used was between 25 and 150 mg/L, the solution pH was 8, and the reaction time was 8 h. The catalyst loading in the solutions was changed to 1 g/L.

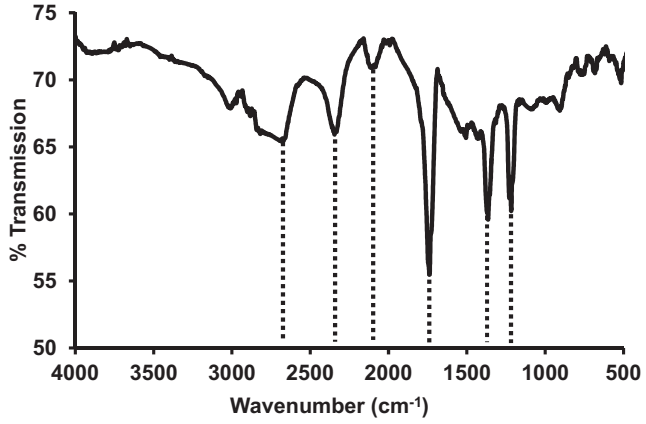

Fig. 2. FTIR spectrum of 40 wt.% titanium dioxide on CNT.

5. Results and discussion

5.1. FTIR analysis on the substrates and TiO_2/CNT nano-composites

The FTIR spectra of the raw MWCNT (not shown) were featureless, whereas the acid treated MWCNT (not shown) had three main absorption peaks at 1203 cm^{-1}, 1353 cm^{-1} and 1745 cm^{-1}. These three peaks are due to the acid treatment procedure, which introduced various oxygen groups onto the surface of the MWCNT. The peak at 1203 cm^{-1} is assigned to a C—O stretch, the peak at 1353 cm^{-1} is due to a nitro group, and the 1745 cm^{-1} peak is assigned to a C=O vibration [17,18].

The CNTs modified with the different loadings of titania were analysed with FTIR and a representative spectrum (the 40 wt.% sample) is presented in Fig. 2. The weak and broad band between 3600 and 4000 cm^{-1} can be assigned to the bending vibrations of co-ordinated water molecules and hydroxyl groups bound to titanium centres (Ti–OH). Between 400–700 cm^{-1} are Ti–O bond vibrations; were rutile phases can occur at 423, 615 and 697 cm^{-1}; and anatase at 514 and 696 cm^{-1} [19,20].

The strong peak at 1217 cm^{-1} can be assigned to a C–O stretch (ether, alcohol, carboxylic acid, or ester); the peak at 1364 cm^{-1} is the nitro group, and the C=O stretch is observed at 1738 cm^{-1}, the peak at 2103 cm^{-1} may be an alkyne group, while the peak at 2345 cm^{-1} is associated with the sorption of CO_2 onto the surface of the TiO_2 (however N_2 also gives a similar band when sorbed onto TiO_2 [21,22]); and the peak at 2684 cm^{-1} remains unassigned. What is interesting to note, is that the 3 main bands observed with the acid-treated CNTs have shifted to higher wavenumbers for the C–O stretch (from 1203 to 1217 cm^{-1}), the nitro group (from 1353 to 1364 cm^{-1}), and to lower wavenumbers with the C=O vibration (1745 to 1738 cm^{-1}) after the deposition of titania. These changes in wavenumbers strongly suggest that some of the titania has adhered to the outer walls of the CNTs, since the change in vibrational energy can be attributed to changes in the local environment brought on by increased mass from the titania deposits. However, no Ti–O–C bonds were formed, since there was no overlap and broadening of the peaks below 1000 cm^{-1} [23,24].

5.2. XRD analysis on TiO_2/CNT samples

Fig. 3(A) presents the results of the XRD analysis on the CNTs before and after acid treatment, and the key CNT peaks were observed at $2\theta = 25.7^\circ$, 42.4°, 53.7° and 78.4°. The peaks were indexed to the hexagonal structure of pure graphite and correspond to the (2 2 0), (1 0 0), (0 0 4) and (1 1 0) reflections respectively

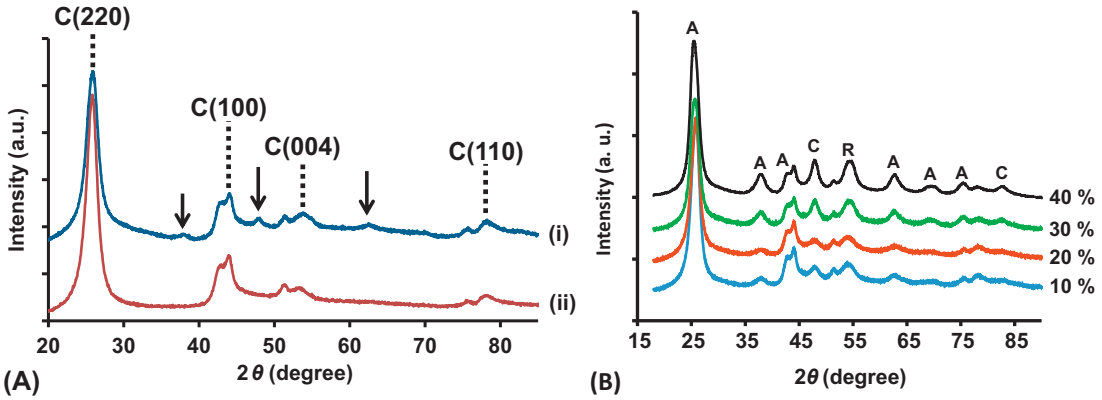

Fig. 3. Panel (A) is the XRD patterns from the untreated and treated MWCNT, arrows indicate metal impurities (iron) peaks; and panel (B) XRD on the 10–40 wt.% TiO_2 on the treated MWCNT, the letters 'A' indicates the anatase phase of titania, 'R' indicates the rutile phase of titania, and the 'C' indicates the graphitic peak of carbon.

[25,26]. The arrows on Fig. 3(A) indicate the peaks for the metal catalyst (iron oxide phase) that was used to synthesize the CNTs, and the absence of those peaks after acid treatment shows that the acid treatment successfully removed a significant amount of residual catalyst.

The different loadings of titania on acid treated CNTs is presented in Fig. 3(B). There was a small increase in the intensity of the titania peaks with an increase in loading, and this is a simple qualitative indication of the change in amount of titania with the samples. The metal oxide was mostly in the anatase phase (Fig. 3B), and the characteristic anatase peaks were identified at $2\theta = 25.9^\circ$, 37.8°, 53.9°. A rutile peak was identified at $2\theta = 65.45^\circ$ and some CNT peaks were observed at $2\theta = 43.2^\circ$, 54.36°, and 77.68°. There were no notable differences between the titania deposited onto the untreated and acid washed CNTs, and this indicates that the residual iron in the CNTs did not affect the formation of the mixed phase anatase. In addition, the main titania peak overlaps with the graphitic carbon peak for CNTs and as a result it is obscured by the titania peak.

The size of the titania nano-particles were calculated using the Scherrer equation and compared with values obtained from HRTEM image analysis and the results are discussed in section 3.4.

5.3. XRD analysis on the TiO_2/CNT samples loaded with noble metals

Fig. 4 compares the XRD patterns for Ag, Pd and Ag/Pd on the 20 wt.% TiO_2/CNT substrate. This particular substrate showed the highest photo-catalytic activity, and thus it was modified with the noble metals. Further discussions on the photo-catalytic activities are presented in the following sections. The CNT graphitic peaks are clearly visible; however, the lowest angle graphitic peak (~25° 2θ) overlays the main anatase peak of the TiO_2. The peaks of the rutile and anatase phases on the composite sample are broadened, which is indicative of smaller particle sizes.

The (1 1 1), (2 0 0) and (2 2 0) reflections of face centred phase of Ag were identified at 38.9, 45.1, and 65.1° 2θ. Palladium peaks at 40, 46.7 and 68.1° 2θ were not easily observed and is due to the small size of the nanoparticles and the dispersion.

6. TEM analysis

All samples were analysed using the TEM, and a representative image of the 20 wt.% sample is presented in Fig. 5.

Although the imaging did not clearly show the titania deposits adhering to the CNTs, SAED analysis (Fig. 5c) revealed diffuse rings and some bright spots that were attributed to the crystalline phases of titania in the sample.

Fig. 6 presents TEM images and STEM images of the various noble metals that were deposited onto the 20 wt.% titania nanocomposites. In the TEM images the noble metal deposits are clearly seen as dark spherical deposits on the samples, while the titania appears as a lower contrast material that can be difficult to distinguish from the CNT support. However, the STEM images not only show the bright and spherical like deposits that are very characteristic of metal nanoparticles, when imaged using the STEM mode, but also the titania appears as low contrast structures that are partially covering the CNTs. Although free deposits of titania were not

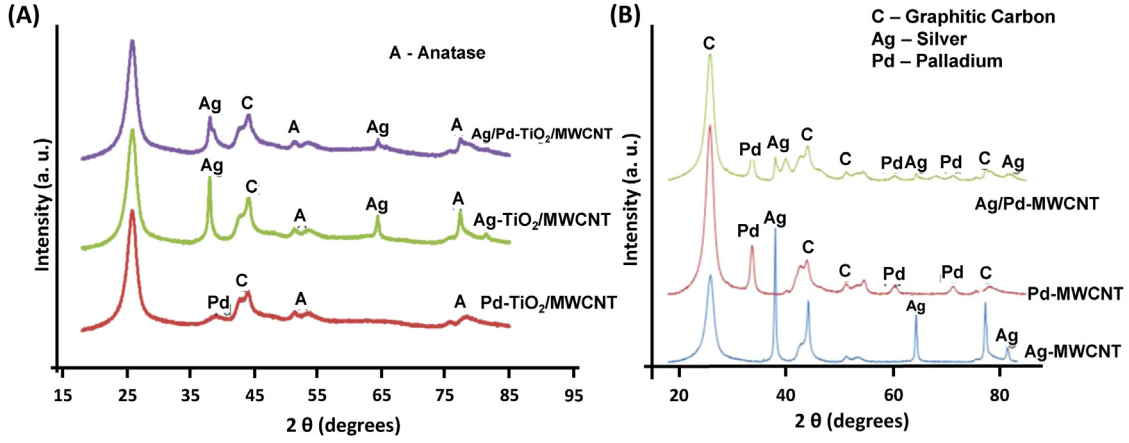

Fig. 4. XRD patterns on (A) Ag, Pd, and Ag/Pd on 20 wt.% TiO_2/CNT and (B) Ag, Pd, and Ag/Pd on untreated CNTs, the metal loading is 2 wt.% for all samples.

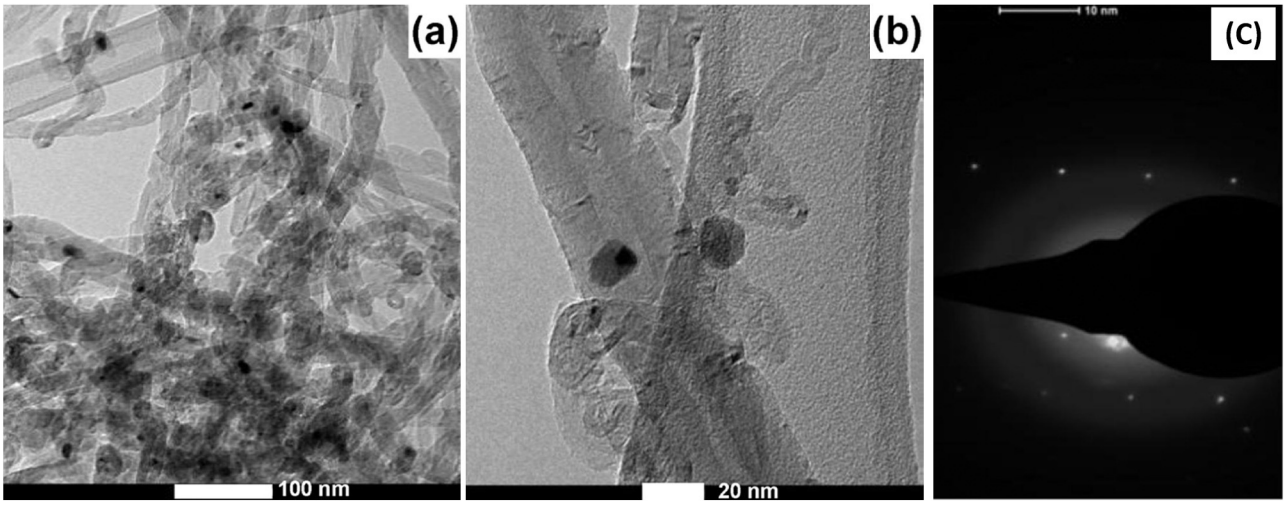

Fig. 5. Representative TEM image of CNTs modified with titania, loading used was 20 wt.%.

Table 1
Average diameter of the respective noble metals deposited onto 20 wt.% titania on CNTs using XRD and TEM image analysis.

Sample	Size of the noble metal nanoparticles from XRD analysis (nm)	Size of the noble metal nanoparticles from TEM analysis (nm)	Weight% of noble metals using EDS
Ag/TiO_2/CNT	3.69	3.44	1.79
Pd/TiO_2/CNT	3.23	3.27	1.84
$Ag\text{-}Pd/TiO_2$/CNT	3.18	3.30	0.93:0.96

observed with the TEM, we cannot discount the possibility that the MOCVD method leads to loose unbound deposits of titania.

The particle size of the various noble metals deposited onto the 20 wt.% titania CNT samples are presented in Table 1. The Scherrer equation was used to calculate the size of the nanoparticles. The peaks used, with the calculation, for the silver and palladium samples were 38.9° and 40.0° 2θ, respectively. 150 nanoparticles were counted for the TEM analysis and the average diameter is reported.

The XRD and TEM analysis are in agreement in terms of the metal palladium forming slightly smaller nanoparticle deposits on the substrates. However the difference in size is relatively small and may not play a significant role in the difference in activity of the photo-catalysts.

The loadings on the various composites were analysed using EDS spot analysis. More than 20 spots per sample were analysed and the average wt% determined and the results are presented in Table 1. The loadings for the titania (not shown) varied between 2 and 4 wt.% below the theoretical loading. The analysis showed a slight variation between the target loadings and measured values. This was in line with our previous work using this method to synthesise nano-composites for fuel cell applications [27].

7. Textural characteristics

Table 2 shows the change in surface area of the samples and a reference sample (commercial titania). Untreated and treated CNTs had a difference in surface area of 26 $m^2\ g^{-1}$, and this can be attributed to the de-bundling of the CNT ropes after the acid treatment and the opening of the CNT end caps thus allowing access to the inner channels. Similar results have been reported elsewhere [28]. The deposition of TiO_2 onto the samples decreased the surface area significantly and this can be attributed to the titania coating the CNTs, and producing a substrate with an overall larger diameter than the original CNTs. The surface area of CNTs has been shown to decrease with increasing diameter of the nanotube [28]. Thus this decrease in surface area can be an indication that the titania deposit has coated the CNTs. However there are other factors that can contribute to the decrease in surface area; such as the blockage of some of the open ends of the CNTs by the titania deposit, or loose low surface area titania deposits mixed with the modified CNTs.

Comparing the TiO_2 loaded samples only (Table 2), the increase observed between the samples with 10 wt.% and 20 wt.% loading was 10 $m^2\ g^{-1}$, while the difference between the samples with 20 wt.% and 30 wt.% loading was 2 $m^2\ g^{-1}$, and between the samples with 30 wt.% and 40 wt.% loading was 4.0 $m^2\ g^{-1}$. These observed changes may be due to a transition from relatively small isolated nanoparticles of titanium dioxide to larger agglomerated nanoparticles. In such a scenario, the deposits on the 10 wt.% and 20 wt.% loaded samples may be dominated by isolated and relatively small nanoparticles on the surface of the MWCNT. However, as the loading was increased from 20–40 wt.%, the nanoparticles were still isolated, but were larger with some agglomerates which may have improved the surface roughness and thus increased the surface area.

In general, when metals were deposited onto the 20 wt.% TiO_2/CNT samples, there was an increase in the surface area from an average value of 97 $m^2\ g^{-1}$ to 142, 124, and 105 $m^2\ g^{-1}$ on the Ag,

Table 2
Surface area of the various samples.

Sample	BET surface area ($m^2\ g^{-1}$)
Commercial TiO_2	17
CNT	131
CNT treated	157
10 wt.% TiO_2/CNT	87
20 wt.% TiO_2/CNT	97
20 wt.% TiO_2/CNT (treated)	143
30 wt.% TiO_2/CNT	99
40 wt.% TiO_2/CNT	103
Ag/TiO_2/CNT	142
Pd/TiO_2/CNT	124
$Ag\text{-}Pd/TiO_2$/CNT	105

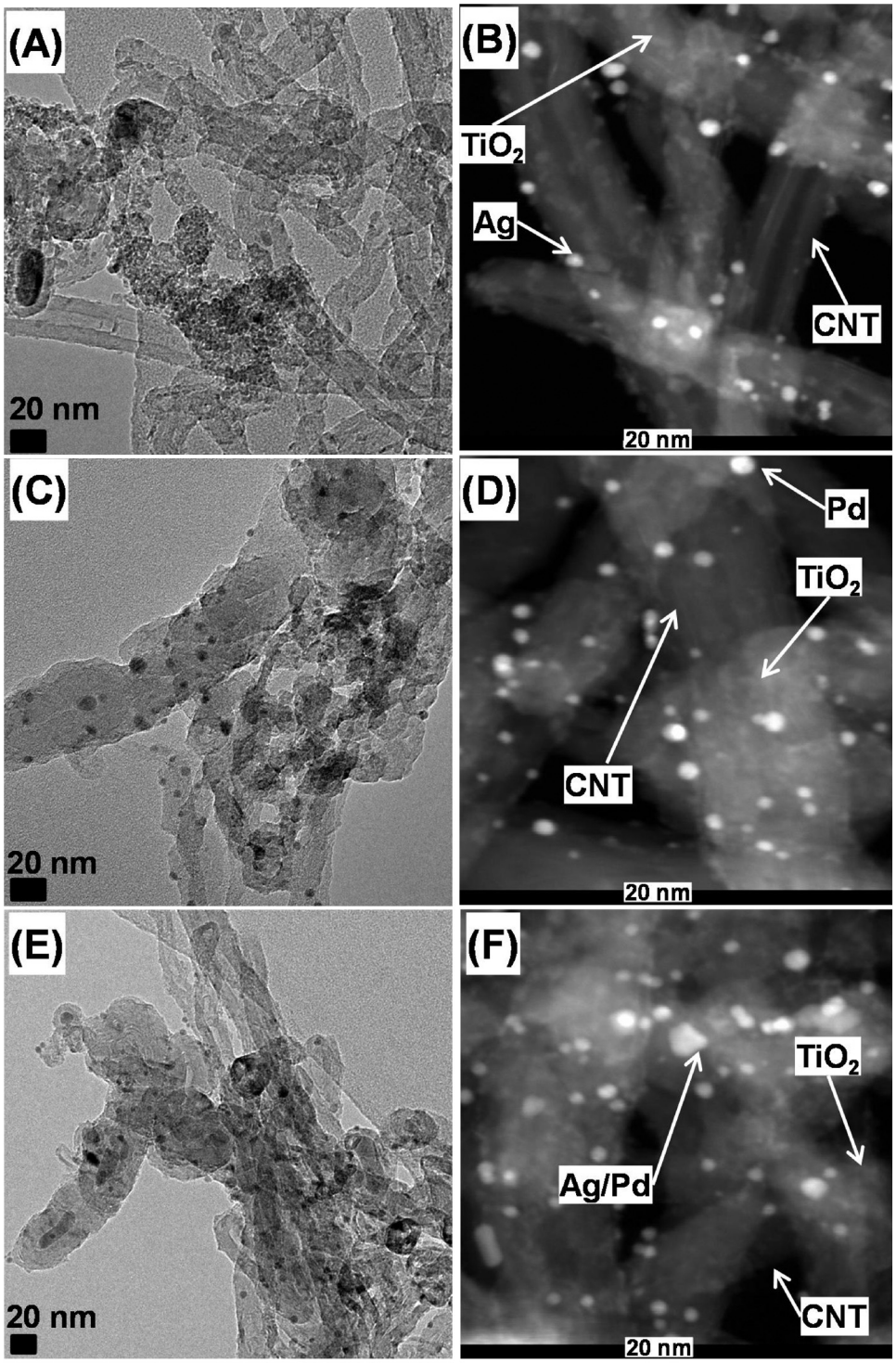

Fig. 6. (A) TEM image of 2 wt.% Ag on 20 wt.% titania on CNT's and corresponding STEM image of the sample is shown in (B); (C) is a TEM image of 2 wt.% Pd on 20 wt.% titania on CNT's and the complimentary STEM image is shown in (D); and finally the sample with 1 wt.% Ag and 1 wt.% Pd, on 20 wt.% titania on CNTs and the samples STEM image in (F).

Pd, and Ag-Pd loaded samples. This can be ascribed to the dispersion of small metal nanoparticles on the surface of the nano-composite. However the decrease from Ag to Pd and the combination of Ag-Pd is unexpected since the XRD and TEM particle size analysis showed that the Pd nanoparticles were smaller than the Ag nanoparticles. Thus we would expect the Pd modified composite to have a larger surface area. As noted above with the titania coatings, a decrease in CNT surface area can be caused by the blockage of some of the open ends on the CNTs [28], and this is the most likely reason with the smaller palladium nanoparticles.

In the CVD process used, a simplistic mechanism includes the precursor transitioning to the gaseous phase on heating, permeating the reactor volume, and then undergoing a decomposition process to form the metal or metal oxide of interest on the CNTs. However, silver acetylacetonate has been shown to start decomposing at temperatures just above 70 °C [29]. Thus, in this

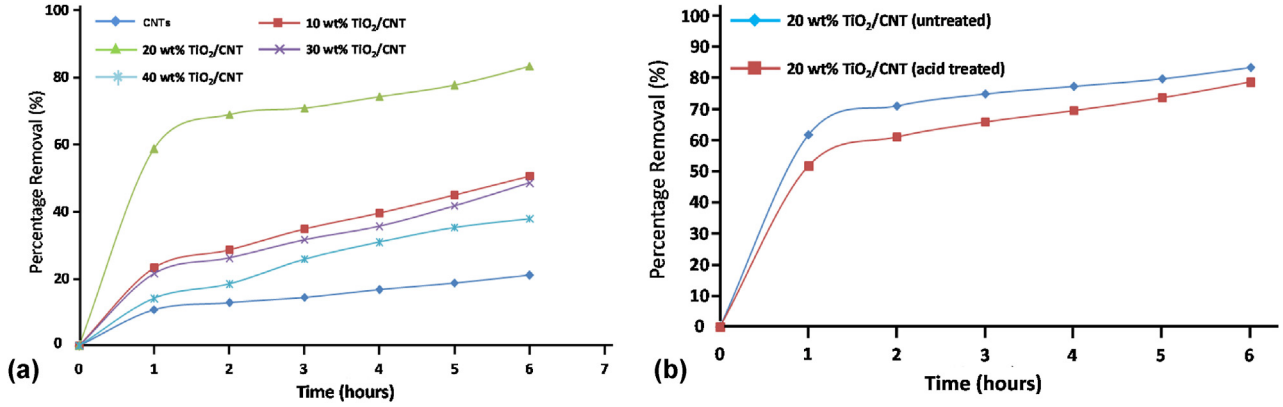

Fig. 7. Panel (a) shows the percentage removal of methylene blue (50 mg/L) versus Time (hours) with the raw CNTs (labeled CNTs), 10, 20 30 and 40 wt.% TiO_2/CNT (1 mg/mL). Panel (b) shows the percentage removal of methylene blue (50 mg/L) versus time (hours) using TiO_2 on treated and untreated CNT samples (1 mg/mL). All samples were run at pH 6.8, 80 rpm, and using the 12 W UV lamp.

process some of the silver begins to deposit on the outside of the titania-CNT nano-composites during the sublimation stage, whereas the more stable palladium acetylacetonate forms a stable vapour phase that can permeate and enter some of the CNT pore openings before decomposition. Pola et al., clearly showed that the thermal stability of silver acetylacetonate increases when mixed with platinum acetylacetonate [29]. With the mixture of Ag and Pd acetylacetonates, we propose a similar phenomenon whereby the palladium acetylacetonate enhances the thermal stability of the silver acetylacetonate, and the two precursors form a stable vapour phase that can lead to the pore blocking that could be occurring with the palladium alone.

8. Photo-catalytic activity

Initial experiments comparing the various loadings of titania on the CNTs with unmodified CNTs are presented in Fig. 7. After 6 h, the removal of methylene blue with CNTs alone was relatively low (20%). The removal increased from 53% to 84% when using the 10 and 20 wt.% TiO_2/CNT respectively. Increasing the loading from 30 to 40 wt.% titania decreased the percentage removal from 51% to 37%.

The activity of the CNTs without TiO_2 can be attributed to the photochemical properties of the surface of the CNTs oxygen containing groups (especially COOH), which have been shown to be active centres for the production of various radical species when CNTs are exposed to light [30–32]. However, we cannot discount a photo-Fenton effect [33,34] from the residual iron that maybe present at the tips of some of the un-treated CNTs or a synergistic effect from the CNTs and residual iron. The result does merit further investigation.

The loading of titania on CNTs is one of a number of parameters that needs to be optimized when synthesising these types of catalysts. With the current CVD system used to synthesize the TiO_2/CNT nano-composites, the increase in the wt.% of titania from 10–20 wt.% resulted in a larger surface area (Table 2), and more photo-active sites for the degradation of methylene blue. With the 30 and 40 wt.% samples, the small increase in surface area is most likely due to additional material depositing onto material already situated on the CNTs, i.e. no significant increase in the dispersion of titania. As a result some of the titania does not take part in the photo-catalytic process and we see a decrease in the activity. Several authors have noted that the amount of titania with or on CNTs can have an effect on the photo-catalytic properties of such types of composites, and our results corroborate these earlier findings [7,23,26,35,36]. The key issue with the different wt.% is the dispersion of the catalyst on the support to ensure maximum synergy between light, catalyst and support. However, another aspect with the nano-composites is the excellent sorption properties of the CNTs, thus too much CNT may result in the target molecule sorbing to the carbon surface without coming into contact with the catalyst, as suggested by some authors [37,38]. One way to account for the overall synergy with the nano-composites is to normalize the first order rate constant with respect to the surface area of the materials. The results are presented in Table 3, and clearly show the 20 wt.% CNT nano-composites to have superior performance when compared to the other samples.

Results presented in Fig. 7(b) show that the acid treatment of MWCNTs prior to deposition of TiO_2 did not improve the photo-catalytic activity of the TiO_2/CNT nano-composites. The untreated TiO_2/CNT nano-composites had a photo-degradation of 83% and the treated samples had a value of 78%.

The optical properties and photoluminescence measurements on the composites are presented in Fig. 8, and are compared with a commercial sample of titanium dioxide (purchased from Sigma-Aldrich). In Fig. 8(a), the commercial sample displays a characteristic absorption peak for titania [26,35,39,40], and the composites show greater absorption of visible light than the commercial titania, and an additional small absorption feature between 440 and 490 nm. Currently, this absorption feature with such composites has not been reported in the literature, and could be due to the resolution of the spectrometer used.

Fig. 8(b) and (c) are Kubelka-Munk plots for the commercial titania sample and the nano-composites. The band gap energies were estimated to be 3.30 eV for the commercial titania, and 2.43, 2.41, 2.40, and 2.43 eV for the 10, 20, 30 and 40 wt.% TiO_2/CNT samples. The difference in the optical properties between titania and the nano-composites can account for the improved photo-catalytic properties of the supported catalysts.

The photoluminescence properties of the nano-composites were compared to that of a commercial sample of titania, and the results are presented in Fig. 8(c). Excitation at 290 nm resulted

Table 3
Rate constant and normalized rate constant for the various photo-catalysts.

Sample	K (min^{-1})	K (min^{-1} m^{-2} TiO_2/CNT)
10 wt.% TiO_2/CNT	0.0888	2.04×10^{-3}
20 wt.% TiO_2/CNT	0.168	3.47×10^{-3}
30 wt.% TiO_2/CNT	0.0835	1.69×10^{-3}
40 wt.% TiO_2/CNT	0.0686	1.33×10^{-3}

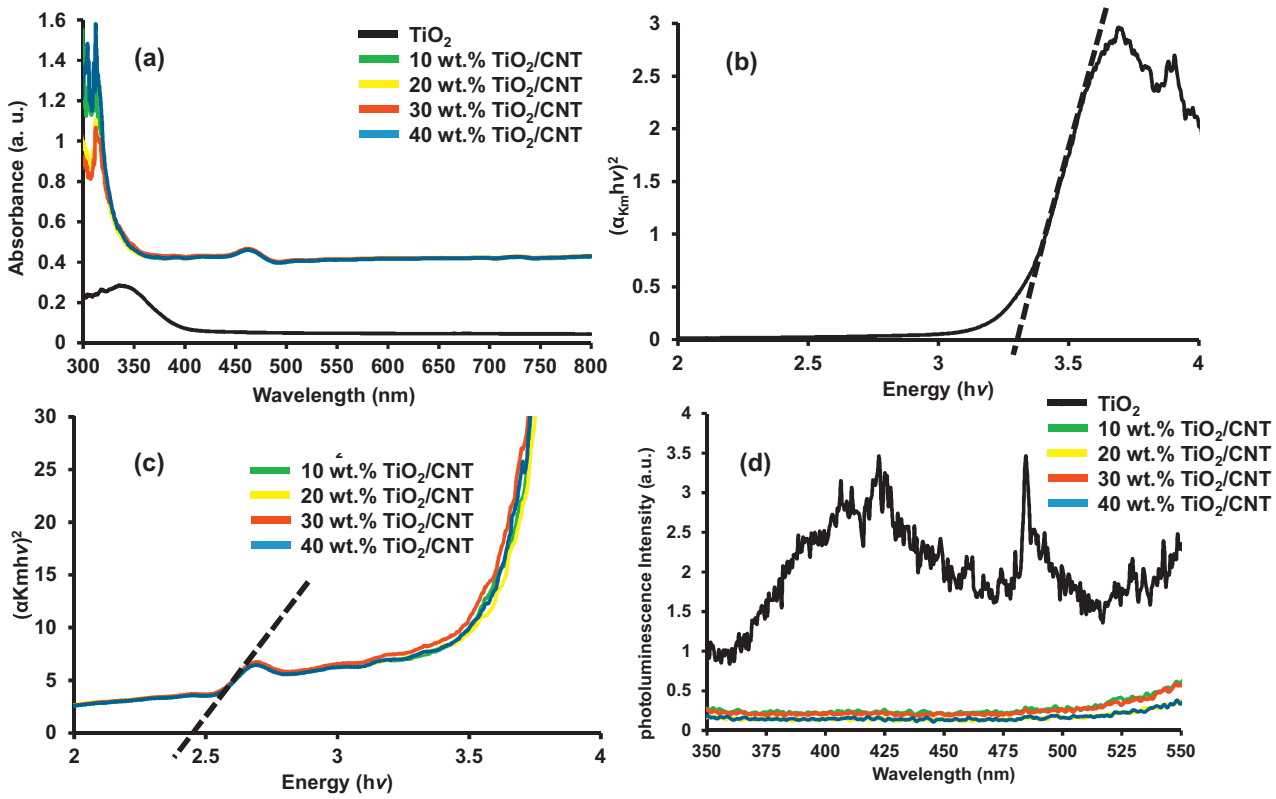

Fig. 8. Panel (a) is the absorption spectra for the TiO_2 nano-composites and a commercial titania powder sample. Panels (b) and (c) are the Kubelka-Munk plots and band gap estimation (direct transition) for titania and the nano-composites. Panel (d) are the photoluminescence spectra of the samples indicated.

in a feature reach PL spectrum for the commercial titania, with a broad peak between 350 and 475 nm and a relatively sharper peak at 485 nm. These features are usually ascribed to the recombination of electrons and holes at surface trap sites on the titania. The absence of the peaks with the nano-composites clearly indicates effective separation of the charge carriers, and that the CNTs in the nano-composites facilitate the movement of photo-excited electrons from the titania. In addition, the PL spectra indicate that the CNTs reduce recombination of electron-hole pairs, and increase the lifetime of the generated holes on the titania [12,35,38,41].

The acid treatment of the CNTs introduced carbon-oxygen groups and nitro groups onto the surface of the CNTs (Fig. 2). These additional defects on the sidewalls of the CNTs have a slight suppression effect on the photo-activity of the composites, by providing trap sites for the photo-generated electrons. This result shows that the introduction of defect sites onto the CNTs should be avoided if possible, and the CVD method used is a viable option for circumventing the sometimes long and lengthy processes for pre-treating CNTs.

8.1.1. The effect of pH on photo-catalytic activity

The pH of the solution affects the sorption of the dye onto the surface of the catalyst, the formation of active radicals in the solution, and to a lesser extent the stability of the suspended catalyst [25]. The continuous agitation during experiments makes the last point irrelevant. The result on how the pH of the system affects the catalyst nano-composite in the degradation of methylene blue is presented in Fig. 9(a).

Although the exact mechanism for the degradation of methylene blue by TiO_2 based photo-catalysts is unknown, it generally involves the formation of O_2 and OH radicals from the electron-hole pairs generated by the TiO_2/CNT composite [12,26,35]. The optimum percentage removal attained at pH 8 can be due to the increased availability of OH^-ions for the formation of OH radicals, and the favourable sorption of the cationic methylene blue dye to the surface of the composites, a similar result was reported by Jiang et al. [11]. However, at higher pH values the percentage removal decreases, even though at high pH values a cationic dye such as methylene blue would favourably sorb onto the surface of the nano-composite. The increase in percentage removal favours the argument that at pH values above 8, the rate of combination between the OH radicals and the excess OH^- ions is greater than the rate at which OH radicals react with dye molecules present in the solution thus lowering the percentage degradation. At acidic pH values, a similar scenario is proposed, whereby the presence of excess H^+ ions combines with the OH radicals thus suppressing the degradation of the dye by the formed radicals.

8.1.2. Comparing treatment time and photo-catalytic activity

Increasing the treatment time increased the percentage degradation of the methylene blue solution (Fig. 9(b)). There was no decrease but a plateau after 10 h. Thus within the time frame used, and with the amounts of catalyst and dye used, there was no inactivation of the catalyst surface.

The lack of catalyst poisoning does suggest it may be possible to use some kind of re-circulating system in which a reasonable surface area of catalyst is exposed to UV light and shorter contact times can be used to degrade the dye i.e. a compact rig as opposed to large area flatbed reactor.

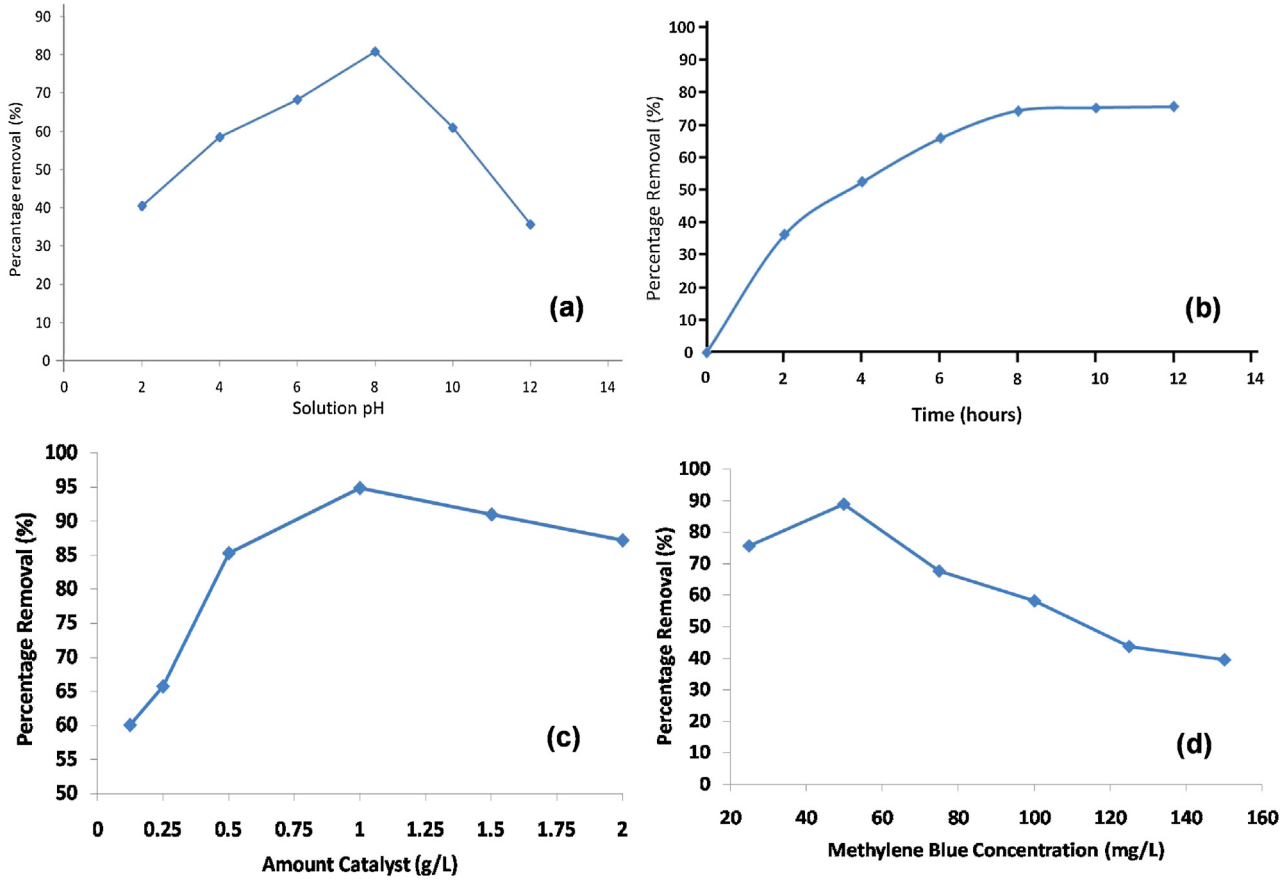

Fig. 9. The graphs show the effect of pH (panel (a) 50 mg/L dye and 1 g/L catalyst), treatment time (panel (b)), amount of catalyst (panel (c) 50 mg/L dye at pH 8.0) and dye concentration (panel (d) 1 g/L catalyst at pH 8.0) on the percentage removal of methylene blue using the 20 wt.% TiO_2/MWCNT (untreated CNT) samples with a stirring rate of 80 rpm, and the 12 W UV lamp.

8.1.3. Results on the variation of amount of catalyst in the solution

The amount of active sites available for the catalytic process is dictated by the surface area of the nano-composite in the solution. Increasing the amount of active sites in the solution i.e. surface area of the nano-composite, will lead to an increase in the percentage degradation, and eventually the degradation rate should show a plateau. This simplistic description assumes a simple pseudo-first order mechanism, and that the rate of generation of the active radical species is the limiting step in the plateau region. However, with photo-catalytic systems the main concern with the amount of catalyst in a batch reactor, such as the one used in this study, is the depth of light penetration. The maximum percentage degradation of methylene blue was observed with 1 g/L of the catalyst in the solution (Fig. 9(c)). The optimum of 1 g/L of the catalyst in the solution is similar to results reported by Sakkas et al. [42]. Since Sakkas et al. [42], used a different dye (congo red) and Degussa P25 catalyst, the similar results do suggest that the light penetration into the solution is a key factor in a batch reactor set-up, and the physical scattering of light by excess solid needs to be optimized.

8.1.4. Varying the concentration of the dye

Methylene blue does absorb in the UV region of the spectrum, thus at high concentration less UV light will reach the active sites of the nano-composite and thus less radicals will be formed for the degradation of the dye. This result was observed when the concentration of the dye was increased from 50 mg/L to 75 mg/L (Fig. 9(d)). At low concentrations of methylene blue, there are active sites of the catalyst still available for the degradation of the dye, thus the limiting step is the movement of dye molecule to the active sites.

8.1.5. Comparing the effect of palladium and silver on the photo-catalytic activity of the nano-composite

Fig. 10(A) shows that the addition of noble metals did improve the photo-degradation activity towards methylene blue. Ag had the highest degradation of 92% in 6 h, palladium had a degradation of 88% in 6 h, but the activity of the bimetallic material resulted in decreased activity, and was recorded at 64%. Ag has been shown to improve the photo-catalytic properties of semiconductor materials, either by improving the separation of charge carriers and reducing the recombination rate of electron hole pairs [43], injection of electrons into the titanium conduction band via a charge transfer mechanism involving surface plasmon resonance phenomenon [44–46], or local electric field enhancement from the plasmonic silver [46]. The use of palladium on the 20 wt.% TiO_2/CNT composite led to a small 5% increase in the removal of methylene blue, and although palladium nanoparticles surface plasmon resonance occurs in UV region of the electromagnetic spectrum [47], the small increase can be attributed to the reduced recombination of electron-hole pairs and not a surface plasmon effect. The larger increase in methylene blue removal with the Ag nanoparticles is attributed to local electric field enhancement from the plasmonic silver, if it were a similar mechanism to that seen with the palladium nanoparticles, we would expect a similar increase, instead of the larger removal of methylene blue observed.

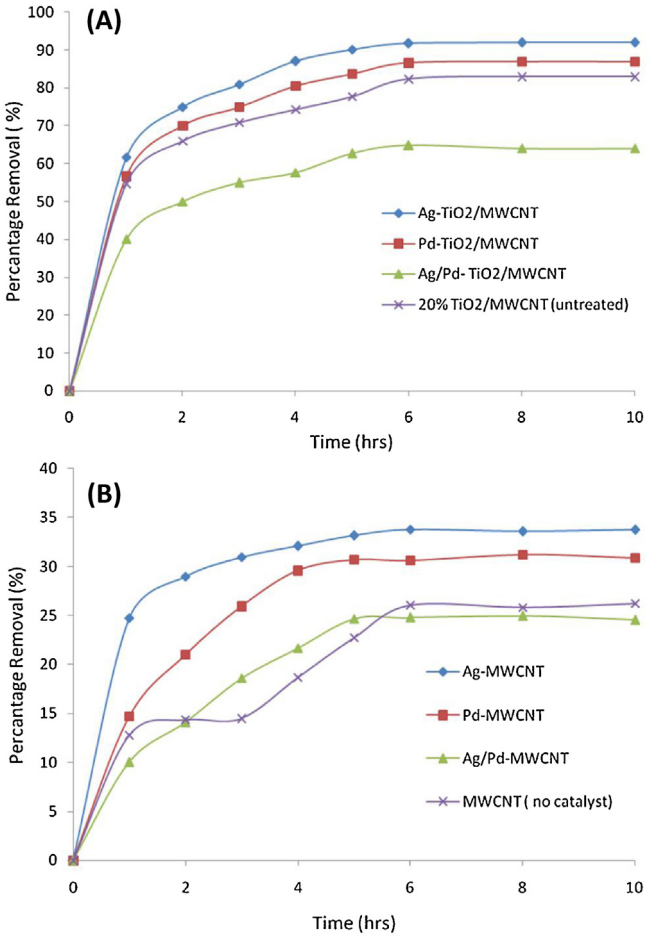

Fig. 10. Comparison of the effectiveness of Ag, Pd, Pd/Ag on TiO_2 on untreated CNT in the photo-degradation of methylene blue.

An unusual result is seen with the bimetallic titania nano-composites, in which the Ag/Pd system supresses the photo-catalytic properties of the titania/CNT system.

Recently, Sun et al. demonstrated that quantum trap depression and charge polarization on Ag/Pd nanoparticles results in the alloy system acting as an electron donor [48]. Thus when used to modify the nano-composite, the alloy increases electron–hole recombination rates by donating excess electrons to the titania material, and as a result we observe a severe reduction in the removal percentage of methylene blue. To the best of our knowledge there is limited information in the open literature where an alloy has been shown to decrease the photo-catalytic activity of titania-CNT composites.

It is interesting to note that the control experiments using CNTs with the various metals and no added TiO_2 did produce some activity Fig. 13(B). This photo-catalytic effect, although small, does highlight the synergistic effect CNTs play in the degradation of the dye.

9. Conclusions

Treated and untreated TiO_2/CNT material at different loadings and noble bimetallic nano-composites (Ag or Pd/- TiO_2/CNT) were synthesized using a MO-CVD method. The XRD results revealed that all the supported TiO_2 consisted of a mixture of anatase, carbon, and a small amount of rutile. The procedure for the MO-CVD metal addition to the substrates did successfully add the desired loading of nano particles of Ag, Pd and Ag/Pd onto the TiO_2 without changing the phase of the TiO_2. The SEM micrographs of TiO_2/CNT composite show the TiO_2 phase is well dispersed onto the CNTs. The EDS analysis confirmed the presence of Ti, C, Ag, Pd and O, while FTIR confirmed the presence of the hydroxyl groups and Ti-O bonds. The catalytic efficiency of the supported nanostructure synthesized was evaluated by photo-degradation studies using methylene blue (MB) as a model pollutant. An optimum loading of 20 wt.% TiO_2/CNT was enough to achieve a degradation rate of 83% in 10 h using 1 g/L of catalyst at pH 8. The deposition of 2 wt.% Ag on 20 wt.% TiO_2/CNT resulted in a greater and faster degradation of MB of 92% in 4 h under the same conditions. It was also shown that the Ag/Pd-TiO_2/CNT photo-catalyst did not improve the photo-catalytic degradation of MB as it only yielded 64% degradation. For metals loaded onto CNTs with no additional TiO_2 33% of the MB was degraded by the Ag/CNT nano-composite, which had the highest activity, and these baseline results confirmed that the TiO_2 is the primary agent for organic pollutant photo-catalytic degradation. The addition of plasmonic Ag enhanced the activity of 20 wt.% TiO_2/CNT by about 10%. This was due to the surface plasmon resonance effect observed with silver, either via an electric field enhancement or a charge transfer mechanism. Therefore, this study presented a highly effective MO-CVD route to prepare quantitative loadings of photo-active materials directly onto a support and demonstrated high photo-catalytic activity of prepared materials.

Acknowledgements

The authors would like to thank IRDP NRF and the Water Research Commission for bursaries and funding; and UWC EMU for assistance with STEM micrographs

References

[1] A. Fujishima, X. Zhang, D.A. Tryk, Surf. Sci. Rep. 63 (2008) 515–582.
[2] U.I. Gaya, A.H. Abdullah, J. Photochem. Photobiol. C 9 (2008) 1–12.
[3] F. Han, V.S.R. Kambala, M. Srinivasan, D. Rajarathnam, R. Naidu, Appl. Catal. A 359 (2009) 25–40.
[4] I.K. Konstantinou, T.A. Albanis, Appl. Catal. B 49 (2004) 1–14.
[5] N. Zhang, Y. Zhang, Y.J. Xu, Nanoscale 4 (2012) 5792–5813.
[6] M.-Q. Yang, Y.-J. Xu, Phys. Chem. Chem. Phys. 15 (2013) 19102–19118.
[7] K. Woan, G. Pyrgiotakis, W. Sigmund, Adv. Mater. 21 (2009) 2233–2239.
[8] Y. Gao, H. Liu, M. Ma, React. Kinet. Catal. Lett. 90 (2007) 11–18.
[9] C.Y. Kuo, J. Hazard. Mater. 163 (2009) 239–244.
[10] Y.-J. Xu, Y. Zhuang, X. Fu, J. Phys. Chem. C 114 (2010) 2669–2676.
[11] G. Jiang, X. Zheng, Y. Wang, T. Li, X. Sun, Powder Technol. 207 (2011) 465–469.
[12] T.A. Saleh, V.K. Gupta, J. Colloid Interface Sci. 371 (2012) 101–106.
[13] S. Takenaka, T. Arike, H. Matsune, M. Kishida, Appl. Catal. B 125 (2012) 358–366.
[14] S.G. Kumar, L.G. Devi, J. Phys. Chem. A 115 (2011) 13211–13241.
[15] A. Kubacka, M. Fernandez-Garcia, G. Colon, Chem. Rev. 112 (2012) 1555–1614.
[16] M.A. Henderson, Surf. Sci. Rep. 66 (2011) 185–297.
[17] L. Stobinski, B. Lesiak, L. Kövér, J. Tóth, S. Biniak, G. Trykowski, J. Judek, J. Alloys Compd. 501 (2010) 77–84.
[18] L. Wang, S. Feng, J. Zhao, J. Zheng, Z. Wang, L. Li, Z. Zhu, Appl. Surf. Sci. 256 (2010) 6060–6064.
[19] L. Castaeda, J.C. Alonso, A. Ortiz, E. Andrade, J.M. Saniger, J.G. Bauelos, Mater. Chem. Phys. 77 (2003) 938–944.
[20] Y. Gao, Y. Masuda, Z. Peng, T. Yonezawa, K. Koumoto, J. Mater. Chem. 13 (2003) 608–613.
[21] C.A. Garćia-González, J. Saurina, J.A. Ayllón, C. Domingo, J. Phys. Chem. C 113 (2009) 13780–13786.
[22] C.N. Rusu, J.T. Yates Jr., J. Phys. Chem. B 105 (2001) 2596–2603.
[23] S. Wang, S. Zhou, J. Hazard. Mater. 185 (2011) 77–85.
[24] S.D. Perera, R.G. Mariano, K. Vu, N. Nour, O. Seitz, Y. Chabal, K.J. Balkus, ACS Catal. 2 (2012) 949–956.
[25] K. Byrappa, A.S. Dayananda, C.P. Sajan, B. Basavalingu, M.B. Shayan, K. Soga, M. Yoshimura, J. Mater. Chem. 43 (2008) 2348–2355.
[26] L. Tian, L. Ye, K. Deng, L. Zan, J. Solid State Chem. 184 (2011) 1465–1471.
[27] Q.-L. Naidoo, S. Naidoo, L. Petrik, A. Nechaev, P. Ndungu, Int. J. Hydrogen Energy 37 (2012) 9459–9469.
[28] J.-P. Tessonnier, D. Rosenthal, T.W. Hansen, C. Hess, M.E. Schuster, R. Blume, F. Girgsdies, N. Pfänder, O. Timpe, D.S. Su, R. Schlögl, Carbon 47 (2009) 1779–1798.
[29] T. Křenek, T. Kovářík, M. Pola, I. Jakubec, P. Bezdička, Z. Bastl, D. Pokorná, M. Urbanová, A. Galíková, J. Pola, Thermochim. Acta 554 (2013) 1–7.
[30] Y.S. Hwang, X. Qu, Q. Li, Carbon 55 (2013) 81–89.
[31] X. Qu, P.J. Alvarez, Q. Li, Environ. Sci. Technol. 47 (2013) 14080–14088.
[32] Y. Zhang, L. Zhou, C. Zeng, Q. Wang, Z. Wang, S. Gao, Y. Ji, X. Yang, Chemosphere 93 (2013) 1747–1754.

[33] E. Casbeer, V.K. Sharma, X.-Z. Li, Sep. Purif. Technol. 87 (2012) 1–14.
[34] Z. Huang, P. Wu, B. Gong, Y. Lu, N. Zhu, Z. Hu, Appl. Surf. Sci. 286 (2013) 371–378.
[35] D. Zhao, X. Yang, C. Chen, X. Wang, J. Colloid Interface Sci. 398 (2013) 234–239.
[36] B. Gao, G.Z. Chen, G. Li Puma, Appl. Catal. B 89 (2009) 503–509.
[37] N. Zhang, Y. Zhang, M.-Q. Yang, Z.-R. Tang, Y.-J. Xu, J. Catal. 299 (2013) 210–221.
[38] Y. Zhang, Z.R. Tang, X. Fu, Y.J. Xu, ACS Nano 5 (2011) 7426–7435.
[39] D. Reyes-Coronado, G. Rodriguez-Gattorno, M.E. Espinosa-Pesqueira, C. Cab, R. de Coss, G. Oskam, Nanotechnology 19 (2008) 145605.
[40] W. Wang, P. Serp, P. Kalck, J.L. Faria, Appl. Catal. B 56 (2005) 305–312.
[41] Y. Zhang, Z.R. Tang, X. Fu, Y.J. Xu, ACS Nano 4 (2010) 7303–7314.
[42] V.A. Sakkas, M.A. Islam, C. Stalikas, T.A. Albanis, J. Hazard. Mater. 175 (2010) 33–44.
[43] D. Zhang, S. Afr. J. Chem. 65 (2012) 98–103.
[44] A. Zielińska, E. Kowalska, J.W. Sobczak, I. Łącka, M. Gazda, B. Ohtani, J. Hupka, A. Zaleska, Sep. Purif. Technol. 72 (2010) 309–318.
[45] Y. Wang, L. Liu, L. Xu, C. Meng, W. Zhu, J. Appl. Phys. 113 (2013) 174311–174317.
[46] W. Hou, S.B. Cronin, Adv. Funct. Mater. 23 (2013) 1612–1619.
[47] S. Jung, K.L. Shuford, S. Park, J. Phys. Chem. C 115 (2011) 19049–19053.
[48] C.Q. Sun, Y. Wang, Y.G. Nie, B.R. Mehta, M. Khanuja, S.M. Shivaprasad, Y. Sun, J.S. Pan, L.K. Pan, Z. Sun, Phys. Chem. Chem. Phys. 12 (2010) 3131–3135.